Antiproton-impact ionization of Ne, Ar, Kr, Xe, and H_2O

I. B. Abdurakhmanov, A. S. Kadyrov, D. V. Fursa, S. K. Avazbaev, J. J. Bailey, and I. Bray
Australian Research Council Centre for Antimatter-Matter Studies, Department of Imaging and Applied Physics, Curtin University, GPO Box U1987, Perth, WA 6845, Australia

(Received 9 January 2015; revised manuscript received 2 February 2015; published 26 February 2015)

We calculate antiproton-impact total single ionization of Ne, Ar, Kr, Xe, and H_2O using a time-dependent convergent close-coupling approach. The Ne, Ar, Kr, and Xe atom wave functions are described in a model of six p-shell electrons above a frozen Hartree-Fock core with only one-electron excitations from the outer p shell allowed. For treating the water molecule we use a neonization method recently proposed by Montanari and Miraglia [J. Phys. B: At. Mol. Opt. Phys. **47**, 015201 (2014)], which describes the ten-electron water molecule as a dressed Ne-like atom in a pseudospherical potential. In the present work the target states of noble gas atoms and water are obtained using a Laguerre basis expansion. For the noble gas atoms there is reasonably good agreement with the calculated single-ionization cross sections.

DOI: 10.1103/PhysRevA.91.022712 PACS number(s): 34.10.+x, 34.50.Gb

I. INTRODUCTION

Ionization of atoms and molecules by fast charged particles is of fundamental interest from practical and theoretical points of view. With the development of sources of low-energy antiprotons, scattering of these antiparticles from atoms and molecules is attracting particular attention; see the review of Kirchner and Knudsen [1]. The Extra Low Energy Antiproton Ring (ELENA) [2] is a small ring at CERN Antiproton Decelerator [3] which will be extended to substantially increase the number of usable (or trappable) antiprotons. The first antiproton scattering experiments with ELENA are planned for 2017. Potential applications of the processes, occurring during antiproton collisions with atoms and molecules, to radiotherapy and oncology (see, e.g., Refs. [1,4]) is another reason for increased interest in antiproton scattering. In addition, understanding of antiproton interactions with atoms and molecules is important to the ALPHA Collaboration at CERN that attempts to test the invariance with respect to charge conjugation, parity transformation, and time reversal (CPT invariance) by forming and trapping antihydrogen [5] and study the gravitational behavior of antimatter at rest [6–8]. Also, the upcoming Facility for Antiproton and Ion Research (FAIR) [9] at Gesellschaft für Schwerionenforschung (GSI) requires the precise knowledge of the collision mechanism between antiprotons and various atomic and molecular targets.

From the theoretical point of view, a number of methods have been developed to model antiproton scattering on light atoms (H and He) and the simplest molecules (H_2^+ and H_2) [1]. More recently, two distinct flavors of the convergent close-coupling (CCC) approach to collisions involving antiprotons have been developed [10–14]. The first version of the CCC approach is a fully quantum-mechanical time-independent method based on the Schrödinger equation for the total scattering wave function and leads to a system of integral equations for transition amplitudes. This approach was applied to antiproton collisions with the H and He atoms [10–12] (and also to the puzzling C^{6+}-He scattering problem [15]). The second, semiclassical, time-dependent version of the CCC approach is based on the Schrödinger equation for the electronic part of the scattering wave function and leads to a set of differential equations. This flavor of the CCC method was applied to antiproton collisions with H_2^+ and H_2 [13,14]. The important feature of the application of the semiclassical time-dependent CCC approach to the antiproton ionization of H_2^+ and H_2 molecules is the ability to account for all possible orientation of the molecular target. The approach significantly improved the agreement between theory and experiment in a wide range of energies of practical interest. In particular, these calculations provided the first quantitative confirmation of the experimentally observed phenomenon of the target-structure-induced suppression of the ionization cross section for low-energy antiproton–molecular hydrogen collisions [16].

Cross sections for ionization of multielectron inert-gas atoms by antiproton impact were measured by Andersen *et al.* [17], Paludan *et al.* [18], and Knudsen *et al.* [19]. There have been a number of calculations performed to study these processes [20–24]. As emphasized in Ref. [1] all of the theoretical approaches are effectively single-electron (hydrogen-atom-like) treatments.

The most sophisticated nonperturbative calculations available for systems with more than two electrons were performed using density-functional theory (DFT) [21,22]. These works investigated single- and multiple-electron processes for medium-energy antiproton collisions with noble gas targets in a semiclassical, time-dependent, independent-particle model (IPM). The model was constructed using the stationary optimized potential method (OPM) of DFT, relying on an accurate description of the target ground state. The OPM method represented the exact exchange-only limit of the exchange-correlation functional of DFT. It was shown that a proper treatment of exchange effects in this model is crucial for the prediction of accurate ionization cross sections. The calculations for ionization of neon and argon targets by antiprotons (and protons) were carried out with frozen target potentials. The frozen target potentials accounted for electronic exchange effects. The single-particle, time-dependent Schrödinger equations from the semiclassical approximation to the collision problem were solved by the so-called basis generator method (BGM). The IPM-BGM approach was applied successfully to calculate integrated ionization cross sections for all processes taking place in antiproton collisions

with noble gases, including single and multiple excitation and ionization of target electrons. In particular, the role of dynamical screening effects was analyzed and a simple model for their inclusion was proposed in the case of antiproton scattering [21,22].

Montanari and Miraglia [23] employed a perturbation continuum-distorted wave-eikonal-initial state (CDW-EIS) approximation to obtain the single- and multiple-ionization probabilities as a function of the impact parameter for antiproton (and proton) impact on rare gas atoms in the energy range from 25 keV to 10 MeV. They included postcollisional electron emission effects believed to be important in the MeV region; however the electron-electron correlations were totally excluded. Despite this they obtained results which seem to agree with the experiment for Ne and Ar better than the IPM-BGM results. Moreover, for the heavier Kr and Xe atoms the agreement appears to become even better.

Knudsen [25] emphasizes the fact that the accuracy with which we are presently able to calculate the outcome of seemingly simple dynamic atomic processes such as single and multiple ionization of few-electron atoms and molecules by charged particle impact is often not better than 10%, and in several cases the uncertainty can even be a factor of two or more. According to Knudsen [25], the reason is not that the participating particles are not well known, nor that the forces between them are in any doubt, but that the many-body nature and especially the electron-electron interaction hinders an accurate calculation for such systems.

The aim of this paper is to present the first multielectron treatment of single ionization in antiproton collisions with noble gas atoms. To this end we further develop the semiclassical, time-dependent CCC method for multielectron targets. The target structure is modeled as six p-electrons above an inert Hartree-Fock core, in the same way as was done for positron scattering [26]. Only one-electron excitations from the outer p-shell are considered. The use of a Laguerre basis makes it possible to take into account all excitation and ionization channels in a systematic manner.

For H_2O we use a neonization method recently proposed by Montanari and Miraglia [24]. This method describes the ten-electron water molecule as a dressed Ne-like atom in a pseudospherical potential. A somewhat similarly effective spherically symmetric potential model was introduced by Lühr and Saenz [27] for the $\bar{p} + H_2$ scattering problem. The neonization method deals with molecules composed by hydrides of the second row of the periodic table of elements: CH_4, NH_3, H_2O, and HF. The method has been tested by calculating ionization cross sections (total, single, and double differential), stopping power, energy-loss straggling, and mean excitation energy. The authors used CDW-EIS, the first-order Born, and the shellwise local plasma approximations. They showed that the neonization model reproduces the various empirical values with high reliability in the intermediate- to high-energy region. In this work we further test the potential of this idea when it is used in the close-coupling formalism.

In the next section we briefly outline the semiclassical impact parameter approach in the context of the convergent close-coupling formalism. Then we present the structure model used to describe the noble gas atoms. Here we also discuss the main ideas of the neonization of the water molecule and provide details of the present implementation in terms of the Laguerre functions. The final section provides details of calculations and presents obtained results.

II. TIME-DEPENDENT CONVERGENT CLOSE-COUPLING METHOD IN IMPACT PARAMETER REPRESENTATION

The time-dependent CCC method has been applied to antiproton-impact ionization of molecular hydrogen [13,14]. Here we generalize it to multielectron targets.

Scattering equations

We consider first antiproton scattering from noble gases and later generalize the method to the water molecule. We use the semiclassical impact-parameter approach. However, the target electrons are treated fully quantum mechanically. The incident antiproton is assumed to be moving with velocity $\boldsymbol{v}$ along a straight-line trajectory $\boldsymbol{R}(t) = \boldsymbol{b} + \boldsymbol{v}t$, where the impact parameter $\boldsymbol{b}$ points along the x axis in the laboratory frame where the target is at rest. The time-dependent, nonrelativistic, Schrödinger equation for the electronic part of the total scattering wave function of a many-body system consisting of the incident antiproton $\bar{p}$ and multiple-electron target is

$$H\Psi(t,\boldsymbol{r},\boldsymbol{R}) = i\frac{\partial\Psi(t,\boldsymbol{r},\boldsymbol{R})}{\partial t}, \tag{1}$$

where $\boldsymbol{R}$ is the position vector of the antiproton relative to the target and $\boldsymbol{r}$ collectively denotes the position vectors of all N target electrons ($\boldsymbol{r} = \{\boldsymbol{r}_1, \ldots, \boldsymbol{r}_N\}$). Since the inclusion of all target electrons is not practically feasible, in what follows only $N = 6$ outermost p-shell electrons of the target will be considered. The total Hamiltonian of the antiproton and target atom scattering system can be written as

$$H = V + H_t, \tag{2}$$

where H_t is the target atom Hamiltonian. The latter can be written in the standard form,

$$H_t = \sum_{i=1}^{N} H_i + \sum_{i<j}^{N} V_{ij}, \tag{3}$$

where H_i is the Hamiltonian of the inert-core+one-electron system (see the next section) and V_{ij} is the Coulomb potential between the outermost p shell electrons. The projectile interaction with the target is written as

$$V = V_0 + \sum_{i=1}^{N} V_{0i}, \tag{4}$$

where V_0 is the interaction of the projectile with the inert core and V_{0i} with the target electrons. The potential V_0 is defined as

$$V_0(R) = -\frac{N}{R} + U_0(R), \tag{5}$$

where

$$U_0(R) = \sum_{\varphi_c}\left(-\frac{1}{R} + \int d^3r' \frac{|\varphi_c(\boldsymbol{r}')|^2}{|\boldsymbol{r}' - \boldsymbol{R}|}\right), \tag{6}$$

where φ_c are inert core orbitals (see below). In the present work we calculated integrated cross sections which do not depend on V_0. Therefore, in the following we ignore this interaction. However, this potential will play an essential role when the method is applied to calculate differential cross sections.

Following the ideas of the convergent close-coupling method we expand the electronic scattering wave function in terms of a certain set of target pseudostates Φ_n according to

$$\Psi(t,\boldsymbol{r},\boldsymbol{R}=\boldsymbol{b}+\boldsymbol{v}t)=\sum_n A_n(t,\boldsymbol{b})\exp(-i\epsilon_n t)\Phi_n(\boldsymbol{r}), \tag{7}$$

where ϵ_n is the energy of the target electronic state n. The expansion coefficients $A_n(t,\boldsymbol{b})$ define the probability for transitions into electronic bound and continuum states.

With this representation of the total scattering wave function the semiclassical Schrödinger equation can be transformed into a set of coupled-channel differential equations for the time-dependent coefficients $A_n(t,\boldsymbol{b})$,

$$i\frac{dA_n(t,\boldsymbol{b})}{dt}=\sum_m A_m(t,\boldsymbol{b})\langle\Phi_n|V(t,\boldsymbol{r},\boldsymbol{b})|\Phi_m\rangle\exp[i(\epsilon_n-\epsilon_m)t]. \tag{8}$$

Equation (8) is solved with the initial conditions $A_n(t=-\infty,\boldsymbol{b})=\delta_{ni}$, as the target is initially in the ground state Φ_i.

III. TARGET STRUCTURE CALCULATIONS

A. Target structure calculations for Ne, Ar, Kr, and Xe

Full details of the target structure calculations for noble gas atoms were given in Ref. [26]. Here we state the main ideas and formulas in order to facilitate calculations of effective potentials in the impact-parameter representation. These are also used when we describe neonization of the water molecule in the following subsection.

We describe wave functions for the noble gases of Ne, Ar, Kr, and Xe by a model of six p-electrons above an inert Hartree-Fock core. Excited states of noble gases are obtained by allowing one-electron excitations from the p-shell. In what follows we consider a more general case of one-electron excitation from a closed-shell atom with the outer shell electron occupying an orbital with angular momentum l_0, with $l_0=1$ being the case for noble gases. This model is similar to the frozen-core model of helium and can be obtained by setting $l_0=0$ in the present formulation. The helium frozen-core model has been used successfully in CCC calculations of electron [28], positron [29], and antiproton [12] scattering on He. This give us confidence in the present approach.

In order to implement this structure model (taking Ne as an example) we conduct calculations in a number of steps. First, we perform self-consistent Hartree-Fock calculations for the Ne^+ ion and obtain a set of orbitals: $1s,2s,2p$. We refer to $1s$ and $2s$ orbitals as inert core orbitals and to the $2p$ orbital as the frozen-core orbital. We then produce a set of Sturmian (Laguerre) functions [30],

$$\xi_{kl}(r)=\left(\frac{2\lambda_l(k-1)!}{(2l+1+k)!}\right)(2\lambda_l r)^{l+1}\exp(-\lambda_l r)L_{k-1}^{2l+2}(2\lambda_l r), \tag{9}$$

where $L_{k-1}^{2l+2}(2\lambda_l r)$ are the associated Laguerre polynomials with λ_l being the fall-off parameter, l is orbital angular momentum, and index k ranges from 1 to N_l, the maximum number of Laguerre functions. This set is used to diagonalize the quasi-one-electron Hamiltonian of the Ne^{5+} ion,

$$H_i=K_i+V_i^{\rm HF}. \tag{10}$$

Here K_i is the kinetic energy operator and $V^{\rm HF}$ is a nonlocal Hartree-Fock potential that is constructed using inert core orbitals φ_c ($1s$ and $2s$ for Ne) according to

$$V^{\rm HF}\varphi(\boldsymbol{r})=-\frac{N}{r}\varphi(\boldsymbol{r})+\sum_{\varphi_c}\left(\int d^3r'\frac{|\varphi_c(\boldsymbol{r}')|^2}{|\boldsymbol{r}'-\boldsymbol{r}|}-\frac{1}{r}\right)\varphi(\boldsymbol{r}) -\sum_{\varphi_c}\int d^3r'\frac{\varphi_c(\boldsymbol{r}')\varphi(\boldsymbol{r}')}{|\boldsymbol{r}'-\boldsymbol{r}|}\varphi_c(\boldsymbol{r}). \tag{11}$$

The result is a set $\{\varphi_\alpha\}$ of one-electron functions that satisfy

$$\langle\varphi_\alpha|H_i|\varphi_\beta\rangle=\epsilon_\alpha\delta_{\alpha,\beta}, \tag{12}$$

where $\delta_{\alpha,\beta}$ is Kronecker δ symbol and ϵ_α is the one-electron energy.

The $2p$ orbital in the $\{\varphi_\alpha\}$ basis differs substantially from the Hartree-Fock $2p$ orbital. In order to build a one-electron basis suitable for the description of a neutral Ne atom we replace the former orbital with the Hartree-Fock one. The basis is then orthogonalized by the Gram-Schmidt procedure. The resulting orthonormal basis is denoted $\{\phi_\alpha\}$ and satisfies

$$\langle\phi_\alpha|H_i|\phi_\beta\rangle=e_{\alpha,\beta}. \tag{13}$$

The coefficients $e_{\alpha,\beta}$ can be trivially obtained from the one-electron energies ϵ_α and overlap coefficients between the Hartree-Fock $2p$ orbital and the $\{\varphi_\alpha\}$ basis.

The target states $\{\Phi_n\}$ of Ne are described via the configuration-interaction (CI) expansion

$$\Phi_n=\sum_\alpha C_\alpha^n\,\tilde{\Phi}_\alpha. \tag{14}$$

The set of configurations $\{\tilde{\Phi}_\alpha\}$ is built by angular momentum coupling of the wave function of $2p^5$ electrons and one-electron functions from the $\{\phi_\alpha\}$ basis. We refer to the former wave function as the frozen-core wave function $\psi_c(l_0^{4l+1})$ and to the latter one as the active electron wave function. The frozen-core wave function has angular momentum l_0 and spin $1/2$, and when coupled with the active electron wave function ϕ_α leads to a configuration with spin $s=0,1$, orbital angular momentum l ($|l_\alpha-l_0|\leqslant l\leqslant l_\alpha+l_0$), and parity $\pi=(-1)^{l_0+l_\alpha}$

$$|\tilde{\Phi}_\alpha\rangle=\mathcal{A}\,\big|l_0^{N-1}:l_0\tfrac{1}{2};l_\alpha:ls\pi\big\rangle, \tag{15}$$

where we used the fact that $N-1=4l_0+1$. The antisymmetrization operator $\mathcal{A}$ is given by

$$\mathcal{A}=\frac{1}{\sqrt{N}}\left(1-\sum_{i=1}^{N-1}P_{iN}\right), \tag{16}$$

where P_{ij} is a permutation operator.

The coefficients C_α^n in the CI expansion Eq. (14) are obtained by diagonalization of the Hamiltonian (3) in the basis of configurations (15). The target orbital angular momentum l,

spin s, and parity π are conserved quantum numbers and diagonalization of the target Hamiltonian is performed separately for each target symmetry $\{l,s,\pi\}$. The resulting set of target states satisfies

$$\langle\Phi_n|H_t|\Phi_m\rangle = \delta_{n,m}\epsilon_n, \tag{17}$$

where ϵ_n is the target-state energy. For antiproton scattering from the ground state ($s = 0$) of a noble gas atom only target states with $s = 0$ can be excited. The size of the calculations can be increased by simply increasing the number of Laguerre functions (N_l). Low-lying states will converge to bound states of the target, while the remaining (pseudo)states will provide an increasingly accurate representation of the target-atom high-lying bound states and an increasingly dense square-integrable representation of the target continuum.

B. Pseudospherical approximation to the water molecule structure

The structure of the water molecule is treated using a neonization idea proposed by Montanari and Miraglia [24]. According to the idea, the water molecule is described as a dressed pseudospherical atom. Following Ref. [24] the multicenter nuclei Coulomb potential of H_2O is approximated with the following spherical potential:

$$V_{H_2O} = -\frac{8}{r} - \frac{2(1-\varepsilon)\Theta(R_H - r)}{R_H} - \frac{2(1-\varepsilon e^{1-r/R_H})\Theta(R_H - r)}{r}, \tag{18}$$

where R_H is the distance between the oxygen atom and either of two hydrogen atoms, Θ is the Heaviside step function, and ε is introduced to account for the deviation of the target potential from spherical symmetry. With a multicenter problem now reduced to a central one we can apply the technique described in the previous section to find energy levels and wave functions. This requires replacing the electron-nuclei term N/r in Eq. (10) with the potential (18). In addition, the $1s$, $2s$, and $2p$ core wave functions for the Ne atom are replaced by corresponding core wave functions for the water molecule. The latter are taken from the Slater basis representation presented in Ref. [24]. Finally, the parameter ε of the potential (18) is varied to match the experimentally measured value for the ground-state energy of the target. As a result the spectrum of the H_2O molecule is represented by the same model as we have used for Ne: six p-electrons above the inert Hartree-Fock core with only one-electron excitations allowed from the closed p shell.

IV. CALCULATION OF THE EFFECTIVE POTENTIALS

Having defined the target structure we can now proceed with the solution of coupled-channel differential equations. The solution strategy is based on the propagation of time-dependent coefficients $A_n(t,\boldsymbol{b})$ starting from $t = -\infty$, where the target is in the ground state, to $t = +\infty$, where, as a result of projectile impact, all changes in the target structure have been established and the projectile no longer feels the Coulomb field of the target center. The time-dependent interaction of the incident projectile with the target is described by the effective matrix elements $\langle\Phi_n|V(t,\boldsymbol{r},\boldsymbol{b})|\Phi_m\rangle$. As mentioned before, for calculations of integrated cross sections, which is the main focus of this paper, it is sufficient to consider the interaction of the projectile with the target electrons only. As the first step we use the CI expansion (14) to express these matrix elements via matrix elements for configurations $\{\tilde{\Phi}_\alpha\}$,

$$\langle\tilde{\Phi}_n|V(t,\boldsymbol{r},\boldsymbol{b})|\tilde{\Phi}_m\rangle = \sum_{\alpha\beta} C_\alpha^n C_\beta^m \langle\tilde{\Phi}_\alpha|V(t,\boldsymbol{r},\boldsymbol{b})|\tilde{\Phi}_\beta\rangle. \tag{19}$$

In order to perform the angular integration in Eq. (19) analytically we use the following multipole expansion of the potential

$$V = \sum_{i=1}^{N}\sum_{\lambda\mu} v_\lambda(R,r_i)Y^*_{\lambda\mu}(\boldsymbol{R})Y_{\lambda\mu}(\boldsymbol{r}), \tag{20}$$

where

$$v_{\lambda\mu}(R,r_i) = -\frac{\min(R,r_i)^\lambda}{\max(R,r_i)^{\lambda+1}}. \tag{21}$$

With this and also using the properties of antisymmetric configurations, Eq. (15), the final expression for the effective matrix elements for configurations $\{\Phi_\alpha\}$ can be written as

$$\langle\Phi_\alpha|V(t,\boldsymbol{r},\boldsymbol{b})|\Phi_\beta\rangle = \sum_\lambda (-1)^{l_m}\frac{1}{\sqrt{2l_m+1}}Y_{\lambda\mu}(\boldsymbol{R})^* C^{l_m m_n}_{l_m m_m \lambda\mu}(I_1(\alpha,\beta,\lambda,R) + I_2(\alpha,\beta,\lambda,R)), \tag{22}$$

where

$$I_1(\alpha,\beta,\lambda,R) = (-1)^{\lambda+l_0+l_\alpha+l_m}\sqrt{(2l_\beta+1)(2l_m+1)}C^{l_\alpha 0}_{l_\beta 0\lambda 0}C^{l_n m_n}_{l_m m_m \lambda\mu}\begin{Bmatrix} l_\beta & l_0 & l_m \\ l_n & \lambda & l_\alpha\end{Bmatrix}\int_0^\infty dr_c r_c^2\varphi_c(r_c)\varphi_c(r_c) \times \int_0^\infty dr_a r_a^2\phi_\alpha(r_a)V_\lambda(r_a,R)\phi_\beta(r_a) \tag{23}$$

and

$$I_2(\alpha,\beta,\lambda,R) = \delta_{l_\alpha l_\beta}\delta_{m_\alpha m_\beta}(-1)^{\lambda+l_\alpha+l_n+1}\sqrt{(2l_0+1)(2l_m+1)}C^{l_0 0}_{l_0 0\lambda 0}C^{l_n m_n}_{l_m m_m \lambda\mu}\begin{Bmatrix} l_0 & l_\alpha & l_m \\ l_n & \lambda & l_0\end{Bmatrix}\int_0^\infty dr_a r_a^2\phi_\alpha(r_a)\phi_\beta(r_a) \times \int_0^\infty dr_c r_c^2\varphi_c(r_c)V_\lambda(r_c,R)\varphi_c(r_c) \tag{24}$$

with $\boldsymbol{R}$, $\boldsymbol{r}_a$, and $\boldsymbol{r}_c$ being the position vectors of the incoming antiproton and the active and core electrons, respectively.

V. CALCULATIONS AND RESULTS

A. Details of calculations

We have performed calculations of antiproton scattering from Ne, Ar, Kr, Xe, and H_2O. Generally, more complex targets (i.e., those with more electrons) require inclusion of higher orbital quantum numbers to get converged results. Specifically, for Ne and Ar the maximum orbital quantum number $l_{\max}$ included were 3 and 5, respectively, while for Kr and Xe $l_{\max} = 9$ was required. This resulted in the number of nl-states being 177, 226, and 377, respectively. Including magnetic quantum numbers the sizes of coupled differential equations for different targets are 803, 1276, and 3475, respectively. For H_2O we use the basis set that was generated for Ne, except that the states of the basis are obtained by diagonalization of the target Hamiltonian containing the Hartree-Fock potential representing the water molecule as a dressed pseudospherical atom.

One measure of the accuracy of the structure model we use in the CCC calculations is the comparison of calculated and observed ionization energies. With aforementioned frozen-core expansions for Ne, Ar, Kr, and Xe we obtain the ionization energies of 20.57, 14.95, 13.38, and 11.73 eV, which agree reasonably with the measured data of 21.56, 16.76, 14.00, and 12.13 eV, respectively. For H_2O, the $2p$-subshell ionization energy in our calculations is the same as the experimentally measured value of 12.6 eV since in our model this energy was used as the empirical parameter to generate the target structure.

Another measure of the target model accuracy is the calculated values for the static dipole polarizability of the target. These values proved to be somewhat larger than the experimentally observed values. This can potentially lead to an overestimation of the calculated cross sections. A simple way to deal with this problem is to introduce a model polarization potential that modifies the dipole term of the electron-electron and antiproton-electron Coulomb potentials. We refer to Ref. [26] for a more detailed discussion and note only that introduction of the model polarization potential allows us to fit calculated polarizability values to the experimental values.

B. Results

The study of ionization cross sections provides a strict test of the theory as it requires an accurate representation of all reaction channels and coupling between them. In Figs. 1–5 we present our calculated total single-ionization cross sections (TSICS) as a function of projectile energy ranging from 5 keV to 2 MeV.

The CCC cross sections for antiproton-impact single ionization of Ne are presented in Fig. 1 in comparison with the experiment and other calculations. As one can see, the present CCC results are in excellent agreement with the experiment at all energies where measurements are available. In this and the following figures we also show our first Born results to indicate the importance of the interchannel coupling. For all considered targets we obtain the expected agreement between the Born results and the experiment at higher projectile energies. Two types of independent particle model calculations of Kirchner *et al.* [21] and CDW-EIS calculations of Montanari and Miraglia [23] yield similar results, which are slightly higher than the experiment. The disagreement systematically increases as the projectile energy decreases. The calculations of Kirchner *et al.* [21], where the time-dependent target screening was included, slightly reduced the cross sections, bringing them closer to the experimental data.

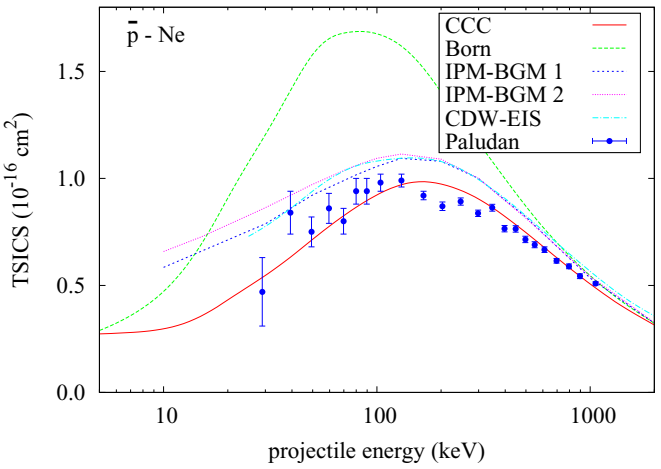

FIG. 1. (Color online) Integrated single-ionization cross section for $\bar{p}$-Ne collisions. The present CCC and Born results are compared with the experimental measurements of Paludan *et al.* [18], independent-particle calculations of Kirchner *et al.* [21,22] with "response" (IPM-BGM 1) and with "no response" (IPM-BGM 2), and CDW-EIS calculations of Montanari and Miraglia [23].

In Fig. 2 we present our results for antiproton-impact single ionization of Ar. At energies above 100 keV and below 1 MeV current results are slightly higher than the experiment and are in good agreement with CDW-EIS calculations of Montanari and Miraglia [23]. Below 50 keV they underestimate

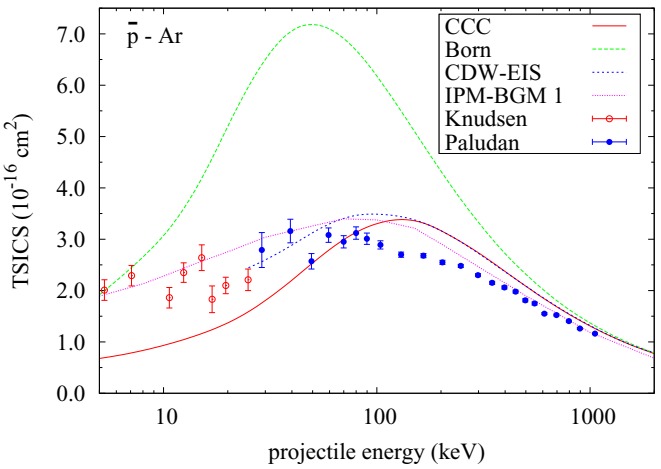

FIG. 2. (Color online) Integrated single-ionization cross section for $\bar{p}$-Ar collisions. Present CCC and Born results are compared with the experimental measurements of Paludan *et al.* [18] and Knudsen *et al.* [19]. Independent-particle calculations of Kirchner *et al.* [21,22] with "response" (IPM-BGM 1) and CDW-EIS calculations of Montanari and Miraglia [23] are also shown.

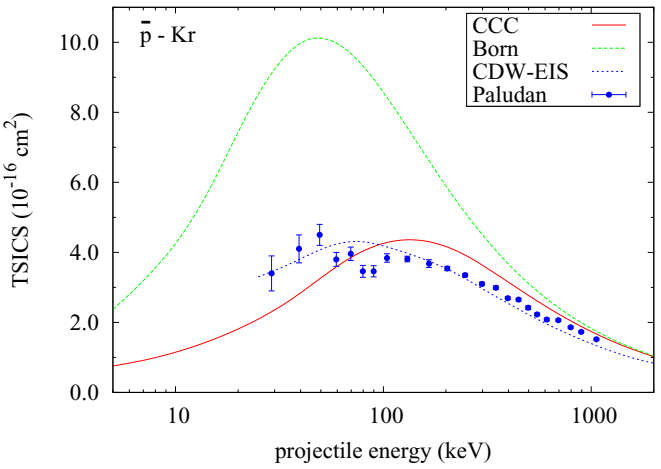

FIG. 3. (Color online) Integrated single-ionization cross section for $\bar{p}$-Kr collisions. Present CCC and Born results are compared with the experimental measurements of Paludan *et al.* [18] and CDW-EIS calculations of Montanari and Miraglia [23].

the experimental data of Paludan *et al.* [18] and Knudsen *et al.* [19]. The measurements for low-impact energies [19] match well with the previous ones by Paludan *et al.* [18] at higher energies. Independent particle model calculations of Kirchner *et al.* [21] where the time-dependent target screening is included better describe the experiment at all energies considered.

The results for ionization of heavier elements by antiproton impact are shown in Figs. 3 and 4. Our calculations for both Kr and Xe yield in general an agreement with the experiment of Paludan *et al.* [18] that is similar to Ar: At high energies calculated curves merge with the measured data; at intermediate energis from 90 to 600 keV they are slightly higher; below 60 keV calculated cross sections fall more rapidly as the impact energy decreases. The CDW-EIS calculations of Montanari and Miraglia [23] describe the experiment very well at all energies. Somewhat unexpectedly,

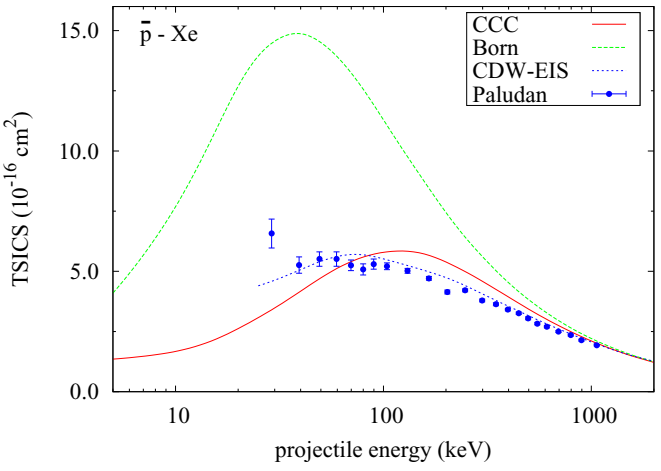

FIG. 4. (Color online) Integrated single-ionization cross section for $\bar{p}$-Xe collisions. Present CCC and Born results are compared with the experimental measurements of Paludan *et al.* [18] and CDW-EIS calculations of Montanari and Miraglia [23].

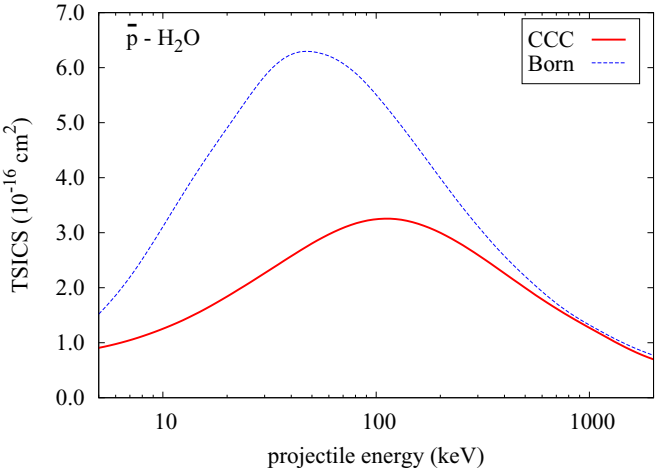

FIG. 5. (Color online) Integrated single-ionization cross section for $\bar{p}$-H_2O collisions. The present CCC and Born results are shown.

for Kr and Xe the agreement between the CDW-EIS results and the experiment is better than for Ne and Ar while the target structure is more complicated.

Finally, the present calculations for single ionization of H_2O by antiproton-impact are shown in Fig. 5. At this stage there are no experimental measurements available for antiproton scattering on the water molecule. However, as we mentioned earlier such experiments are planned for the near future. We expect that since the current results were obtained using the nonperturbative, close-coupling approach they should be reliable at energies down to 1 keV. This should provide guidance to future experiments.

VI. CONCLUSIONS

We have presented antiproton-impact single-ionization of Ne, Ar, Kr, Xe, and H_2O using a time-dependent convergent close-coupling approach. For the description of Ne, Ar, Kr, and Xe atom wave functions, we used a model of six p-shell electrons above an inert Hartree-Fock core with only one-electron excitations from the outer p-shell allowed. The water molecule is treated using a neonization model recently proposed by Montanari and Miraglia [24]. This model describes the ten-electron water molecule as a dressed atom in a pseudospherical potential like Ne. For all targets considered in the present work the expansion basis is obtained using the orthogonal Laguerre functions. Calculated single-ionization cross sections for Ne, Ar, Kr, and Xe are in good agreement with the experimental measurements. A common feature of the CCC cross sections for the noble gas targets is that they underestimate the experimental data below 100 keV and slightly overestimate them above this energy. Since we use the frozen-core approximation for the target structure, this is to be expected. Our previous calculations of antiproton-impact ionization of He [12] where the target structure was treated using both frozen-core and multiconfiguration approximations showed that the total ionization cross sections obtained in the multiconfiguration treatment were substantially higher at the lower energies (below 100 keV) than the frozen-core ones and slightly higher at the higher energies. This

suggests that for a better agreement with experiment a proper multiconfigurational treatment of the many-electron target is required. Finally, the agreement between our present results for the heavier noble-gas targets and experiment is slightly worse than for the lighter targets. Apart from the frozen-core approximation, heavier targets like Xe may require a relativistic treatment.

ACKNOWLEDGMENTS

We thank Claudia Montanari and Tom Kirchner for providing their data in tabulated forms. The work is supported by the Australian Research Council and the Australian National Computational Infrastructure Facility and its Western Australian node iVEC.

[1] T. Kirchner and H. Knudsen, J. Phys. B: At. Mol. Opt. Phys. **44**, 122001 (2011).
[2] Extra Low Energy Antiproton Ring, espace.cern.ch/elena-project
[3] The Antiproton Decelerator, home.web.cern.ch/about/accelerators/antiproton-decelerator
[4] N. Bassler, J. Alsner, G. Beyer, J. J. DeMarco, M. Doser, D. Hajdukovic, O. Hartley, K. S. Iwamoto, O. Jkel, H. V. Knudsen, S. Kovacevic, S. P. Mller, J. Overgaard, J. B. Petersen, T. D. Solberg, B. S. Srensen, S. Vranjes, B. G. Wouters, and M. H. Holzscheiter, Radiother. Oncol. **86**, 14 (2008).
[5] C. Amole *et al.* (ALPHA Collaboration), Nature (London) **483**, 439 (2012).
[6] ALPHA Collaboration and A. E. Charman, Nat. Commun. **4**, 1785 (2013).
[7] A. Kellerbauer *et al.* (AEGIS Collaboration), Nucl. Instr. Meth. B **266**, 351 (2008).
[8] P. Debu *et al.* (GBAR Collaboration), Hyperfine Interact. **212**, 51 (2012).
[9] Facility for Antiproton and Ion Research, www.fair-center.org
[10] I. B. Abdurakhmanov, A. S. Kadyrov, I. Bray, and A. T. Stelbovics, J. Phys. B: At. Mol. Opt. Phys. **44**, 075204 (2011).
[11] I. B. Abdurakhmanov, A. S. Kadyrov, I. Bray, and A. T. Stelbovics, J. Phys. B: At. Mol. Opt. Phys. **44**, 165203 (2011).
[12] I. B. Abdurakhmanov, A. S. Kadyrov, D. V. Fursa, I. Bray, and A. T. Stelbovics, Phys. Rev. A **84**, 062708 (2011).
[13] I. B. Abdurakhmanov, A. S. Kadyrov, D. V. Fursa, and I. Bray, Phys. Rev. Lett. **111**, 173201 (2013).
[14] I. B. Abdurakhmanov, A. S. Kadyrov, D. V. Fursa, S. K. Avazbaev, and I. Bray, Phys. Rev. A **89**, 042706 (2014).
[15] I. B. Abdurakhmanov, I. Bray, D. V. Fursa, A. S. Kadyrov, and A. T. Stelbovics, Phys. Rev. A **86**, 034701 (2012).
[16] H. Knudsen, H. A. Torii, M. Charlton, Y. Enomoto, I. Georgescu, C. A. Hunniford, C. H. Kim, Y. Kanai, H.-P. E. Kristiansen, N. Kuroda, M. D. Lund, R. W. McCullough, K. Tökesi, U. I. Uggerhøj, and Y. Yamazaki, Phys. Rev. Lett. **105**, 213201 (2010).
[17] L. H. Andersen, P. Hvelplund, H. Knudsen, S. P. Moller, A. H. Sorensen, K. Elsener, K.-G. Rensfelt, and E. Uggerhoj, Phys. Rev. A **36**, 3612 (1987).
[18] K. Paludan, H. Bluhme, H. Knudsen, U. Mikkelsen, S. P. Mller, E. Uggerhj, and E. Morenzoni, J. Phys. B: At. Mol. Opt. Phys. **30**, 3951 (1997).
[19] H. Knudsen, H.-P. E. Kristiansen, H. D. Thomsen, U. I. Uggerhøj, T. Ichioka, S. P. Møller, C. A. Hunniford, R. W. McCullough, M. Charlton, N. Kuroda, Y. Nagata, H. A. Torii, Y. Yamazaki, H. Imao, H. H. Andersen, and K. Tökesi, Phys. Rev. Lett. **101**, 043201 (2008).
[20] T. Kirchner, L. Gulyás, H. J. Lüdde, E. Engel, and R. M. Dreizler, Phys. Rev. A **58**, 2063 (1998).
[21] T. Kirchner, H. J. Lüdde, and R. M. Dreizler, Phys. Rev. A **61**, 012705 (1999).
[22] T. Kirchner, M. Horbatsch, and H. J. Lüdde, Phys. Rev. A **66**, 052719 (2002).
[23] C. C. Montanari and J. E. Miraglia, J. Phys. B: At. Mol. Opt. Phys. **45**, 105201 (2012).
[24] C. C. Montanari and J. E. Miraglia, J. Phys. B: At. Mol. Opt. Phys. **47**, 015201 (2014).
[25] H. Knudsen, J. Phys.: Conf. Ser. **194**, 012040 (2009).
[26] D. V. Fursa and I. Bray, New J. Phys. **14**, 035002 (2012).
[27] A. Lühr and A. Saenz, Phys. Rev. A **78**, 032708 (2008).
[28] D. V. Fursa and I. Bray, Phys. Rev. A **52**, 1279 (1995).
[29] R. Utamuratov, A. S. Kadyrov, D. V. Fursa, and I. Bray, J. Phys. B: At. Mol. Opt. Phys. **43**, 031001 (2010).
[30] I. Bray, Phys. Rev. A **49**, 1066 (1994).